THE JOURNAL OF PHYSICAL CHEMISTRY B

ARTICLE

pubs.acs.org/JPCB

Assembly of Bioactive Peptide−Chitosan Nanocomplexes

B. Hu,[†,‡] S. S. Wang,[‡] J. Li,[†] X. X. Zeng,[‡,*] and Q. R. Huang[†,*]

[†]Department of Food Science, Rutgers University, 65 Dudley Road, New Brunswick, New Jersey 08901, United States

[‡]College of Food Science and Technology, Nanjing Agricultural University, Nanjing 210095, People's Republic of China

ABSTRACT: The assembly of nanocomplexes from bioactive peptides, namely, caseinophosphopeptides (CPPs) and chitosan (CS), at physiological conditions and various CS/CPP mass ratios has been systematically studied using a combination of liquid chromatography−tandem mass spectrometry (LC−MS/MS), turbidimetric titration, dynamic light scattering (DLS), electrophoretic mobility (ζ-potential) measurements, transmission electron microscopy (TEM), and fluorescence spectroscopy. Peptides incorporated with CS forming nanoparticles were prepared and identified using LC−MS/MS. They were characterized by different amounts of clusters of phosphorylated seryl residues. At low salt concentrations, an increase in CS/CPP mass ratio shifted the critical $pH_{\varphi 1}$ value, which was designated as the formation of CS/CPP nanocomplexes, as well as pH_{max}, which represents the neutralization of positive and negative charges at higher pH values. The sizes, charges, morphologies, binding mechanisms, and binding constants of the bioactive peptide−chitosan nanocomplexes were analyzed, and our results suggest that three processes are involved in nanocomplex formation: First, negatively charged CPPs absorb to positively charged CS molecular chains to form intrapolymer nanocomplexes saturated with CPPs (CPPNPs). Subsequently, the negatively charged CPPNPs are bridged by the addition of positively charged CS, resulting in the formation of nearly neutral associative biopolymer complexes. Finally, further addition of excess chitosan breaks down the bridges of associative complexes and causes the formation of positively charged isolated spherical nanocomplexes. The binding between the peptides and CS is mainly driven by electrostatic interactions with a binding constant of $K_{cs} = 4.6 \times 10^4\ M^{-1}$. Phosphorylated groups and other negatively charged amino acids, such as aspartic acid (Asp) and glutamic acid (Glu), in the CPPs might be the dominant sites for interaction with $-NH_3^+$ groups on the CS molecular chains.

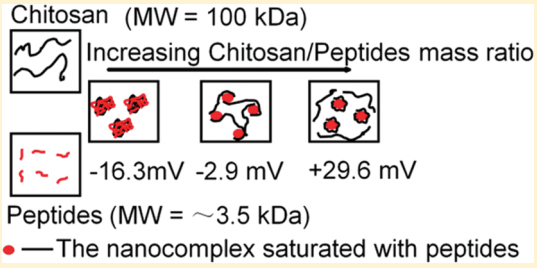

INTRODUCTION

Recently, significant efforts have been directed toward the investigation of the assembly of polyelectrolytes and proteins forming different hierarchical supramolecular structures on length scales from nanometers to micrometers, such as coacervates, multilayers, and brushes.[1−3] Such structures have been applied to the development of drug delivery systems for macromolecules, such as proteins, peptides, and genes. Among these structures, nanospheres represent a new group of carrier particles for enzymes and proteins.[2,4] A number of noncovalent forces can contribute to complex formation between different polymers, including proteins and polysaccharides, and the predominance of electrostatic interactions is widely accepted. Voorn−Overbeek and Veis−Aranyi theories, as well as their derivatives, have already been used to interpret the mechanism of interactions between different polymers, including proteins and polysaccharides.[3,5] However, detailed information about the interactions between polyelectrolytes and natural peptides, which are constituent elements of a protein, and the corresponding interaction models have scarcely been reported.[6,7] In fact, complexes containing bioactive polymers have attracted great interest, which also provides an approach to investigate the relationship between structure and biological activity.[8−10]

Biopolymers of food origin are fascinating and important materials, making up some of the most complex examples of soft condensed matter (SCM) with which people interact daily.[11] They are natural sources of biopolymeric soft materials and are not only biodegradable and biocompatible, but also biofunctional.[12,13] Many peptides from plants and animals with relevant bioactive potential have been discovered, with the majority being isolated from milk-based products.[14] Tryptic digestion of the casein proteins yields caseinophosphopeptides (CPPs) from the N-terminal polar region, which contain clusters of phosphorylated seryl residues.[15] CPPs reveal multifunctional bioactivities. They can form soluble organophosphate salts and function as carriers for different minerals, especially calcium, zinc, and iron, to enhance mineral absorption/bioavailability in the small intestine.[16] Cross et al. characterized the physicochemical properties of casein phosphopeptide−amorphous calcium phosphate nanocomplexes.[17] Laparra et al. reported that CPPs can protect against hydrogen peroxide-(H_2O_2-) induced oxidative stress in human intestinal epithelial Caco-2 cells.[18] Furthermore, CPPs have been shown to exert cytomodulatory effects, inducing apoptosis of cancer cells[19] and stimulating the activity of immunocompetent cells and neonatal intestinal cells.[20]

Received: February 10, 2011
Revised: April 20, 2011
Published: May 24, 2011

Chitosan (CS) is composed of glucosamine, known as 2-amino-2-deoxy-(1 → 4)-β-D-glucopyranan. It is the deacetylated form of chitin and is considered the most widely distributed cationic biopolymer. CS is a nontoxic, biodegradable, and biocompatible polyelectrolyte. Moreover, it exhibits antimicrobial and antitumor activities.[21,22] Because of their subcellular and submicrometer size, CS nanoparticles can penetrate deep into tissues through fine capillaries and cross the fenestration present in the epithelial lining. This allows efficient delivery of therapeutic agents to target sites in the body.[23,24]

In this work, CPPs were prepared by the tryptic digestion of bovine casein proteins and separated by selective precipitation and anion-exchange column. The chemical structures of the CPPs arising from binding to CS were identified using liquid chromatography−tandem mass spectrometry (LC−MS/MS) combined with database searching. The interactions between CS and CPPs as a function of pH at different mass ratios were monitored by turbidimetric titration, dynamic light scattering (DLS), and ζ-potential measurements, whereas the morphology of the nanoscaled spherical polysaccharide−peptide complexes was monitored by transmission electron microscopy (TEM). Quenching of the intrinsic tryptophan (Trp) fluorescence of CPPs was used as a tool to study the interactions of CS with CPPs in an attempt to characterize the nature of the polymer−peptide complexation. Finally, a model for the interaction between the bioactive peptides and chitosan at low salt concentration is also presented.

EXPERIMENTAL METHODS

Materials. Bovine casein of technical grade was purchased from Sigma Co. (St. Louis, MO). Trypsin was obtained from Sinopharm Chemical Reagent Co. (Shanghai, China). The CPPs were prepared as described in the next section. Chitosan (CS) with a molecular weight of 100 kDa was obtained from Golden-Shell Biochemical Co. Ltd. (Hangzhou, China). The degree of deacetylation was 90%. High-performance-liquid-chromatography- (HPLC-) grade of acetonitrile (MeCN) and formic acid were purchased from Fisher Scientific (Pittsburgh, PA). Other chemicals were of reagent grade and were used without further purification.

Hydrolysis and Preparation of CPPs. The CPPs were prepared according to a previously reported method[25] with modifications. Fifty grams of bovine casein was dissolved in 500 mL of 0.05 M NaOH solution with gentle stirring to produce a 10% (w/v) solution. The pH of the solution was adjusted to 8.00. Then, 0.25 g of trypsin was dissolved in 7.5 mL of distilled water immediately before addition to the casein solution in order to avoid extensive self-hydrolysis. Hydrolysis was carried out under gentle agitation at constant temperature (50 °C) and constant pH (8.00), controlled by neutralization of the released hydrogen ions using 1 M NaOH. The hydrolysis proceeded until base consumption ceased, at which point the hydrolysis was considered complete. The trypsin was inactivated by heating the crude hydrolysate to 80 °C and holding this temperature for 5 min. The crude hydrolysate was subjected to selective precipitation of hydrophobic peptides by adjusting the temperature to 40 °C and the pH to 4.60 using concentrated hydrochloric acid. After 1−2 h of flocculation, the precipitate was separated from soluble peptides by centrifugation at 2000 rpm for 30 min. The suspension of soluble peptides (F_1) was collected for further purification. Before separation through an anion-exchange column, F_1 was adjusted to pH 8.9 with 2 M sodium hydroxide to generate F_2. The soluble peptide solution F_2 was loaded onto a HiPrep column (16/10 QXL, Amersham Biosciences, Piscataway, NJ) pre-equilibrated with 20 mM (pH 8.9) tris(hydroxymethyl)aminomethane hydrochloride (Tris-HCl) buffer (mobile phase A) for five column volumes at a flow rate of 5.0 mL/min. After elution with mobile phase A for 10 min, the column was eluted with 20 mM (pH 8.9) Tris-HCl buffer with 1 M NaCl (mobile phase B) at a flow rate of 5.0 mL/min. The elution was monitored by measuring the absorbance at 280 nm and autocollected at 5 mL/tube. The eluted fractions were collected, evaporated by a rotary evaporator at 40 °C (Heidolph Laborota 4000 efficient, Schwabach, Germany), dialyzed to desalinate, and lyophilized by a Labconco Freeze-Dry System (Labconco Corp.) to give the CPP sample.

Identification of the Peptide Structure by LC−MS/MS. *Preparation of the Peptide Sample.* The peptide/polysaccharide nanosuspension was centrifuged at 20000*g* for 30 min. The supernatant was discarded. The precipitate of nanoparticles was washed with 10 μM Tris-HCl buffer with 0.01 M NaCl (pH 6.0) three times. Then, the precipitate of peptide−polysaccharide nanoparticles was dissociated with pH 2.5 HCl solution. After being filtered through 0.45-μm Whatman filters, the solution was loaded onto the LC−MS/MS instrument.

LC−MS Analysis. Each sample was analyzed by nanospray LC−MS/MS using an LC-Packings HPLC instrument coupled to an LTQ-Velos-Orbitrap mass spectrometer. The LC gradient was 2−45% acetonitrile in 0.1% formic acid in 27 min at a flow rate of 250 nL/min. MS spectra were acquired in orbitrap over the range m/z 300−2000 with a resolution of 60000. The top 20 most intense precursor ions were subjected to MS/MS analysis in an ion trap with dynamic exclusion set to repeat each MS/MS analysis twice within 30 s and to exclude the same mass for 60 s thereafter.

Mascot Database Search. Peak lists were generated using Proteome Discoverer software. The data were searched against Swiss-Prot database using Mascot 2.2 with following parameters: no enzyme, variable modifications of oxidation (Met) and phosphorylation (STY), and mass error tolerances of ±10 ppm for MS and ±0.6 Da for MS/MS.

Turbidimetric Titrations. pH-dependent turbidity measurements, reported as 100 − T (%), were carried out at a light wavelength of 420 nm using a Brinkmann PC910 colorimeter equipped with a 1-cm-path-length optical probe. The colorimeter was calibrated to read 100% transmittance with Milli-Q water. CS was dissolved in 1% (w/v) acetic acid solution with 0.01 M NaCl until the solution was transparent. The CPP solution prepared in 0.01 M NaCl was adjusted to pH 2.5. All solutions were filtered using 0.45-μm Whatman filters prior to use. NaOH solution (suitable concentration) was used to adjust the pH of a mixture containing equal volumes of 0.5 mg/mL CPPs and CS with varying concentrations (0, 0.0625, 0.125, 0.25, 0.5, and 1.0 mg/mL) under gentle stirring. After the addition of each small droplet of HCl, the turbidity value was collected, and the pH was monitored with a Thomas Scientific pH meter (model 8025) calibrated with two buffers of pH 4 and 7. All measurements were conducted at 25 °C. In addition, the pH-dependent turbidities of mixed solutions of 0.5 mg/mL CPP and 0.1 mg/mL CS in 0.01, 0.05, and 0.1 M NaCl were also recorded according to the same method.

Preparation of Stock Solution. CS solution (8 mg/mL) with 0.02 M NaCl was adjusted to pH 6.0. Then, equal volumes of the

8 mg/mL CS solution and 20 mM (pH 6.0) Tris-HCl buffer were mixed to form pH 6.0 CS stock solution. CPPs were dissolved in 10 mM (pH 6.0) Tris-HCl buffer with 0.01 M NaCl.

Preparation of Nanocomplex. Equal volumes of CS and CPP solutions with different CS/CPP mass ratios were mixed together with stirring at room temperature. The formation of CS−CPP nanoparticles started spontaneously by the CPP-initiated ionic gelation mechanism.

Dynamic Light Scattering (DLS). The mean particle sizes and size distributions were determined using a dynamic-light-scattering-based BIC 90 plus particle size analyzer equipped with a Brookhaven BI-9000AT digital correlator (Brookhaven Instrument Corporation, New York) at a fixed scattering angle of 90° at 25 ± 1 °C. The light source was a solid-state laser operating at a wavelength of 658 nm with 30 mW power, and the signals were detected by a high-sensitivity avalanche photodiode detector. The change of the particle sizes and polydispersities with different polysaccharide/peptide mass ratios was studied. The DLS autocorrelation functions were analyzed by the well-known cumulant method,[26] where the field−field autocorrelation $g(q,t)$ was decomposed into a distribution of decay rates Γ (= $1/\tau$) given by

$$g(q,t) = \int G(\Gamma)\mathrm{e}^{-\Gamma t}\,\mathrm{d}\Gamma \quad (1)$$

The first two moments of the distribution G(Γ) are

$$\Gamma = Dq^2 \quad (2)$$

$$\mu_2 = (D^2 - D^{*2})q^4 \quad (3)$$

where D^* is the average diffusion coefficient and q is the amplitude of the scattering vector. The polydispersity term defined in the cumulant analysis is

$$\text{polydispersity} = \mu_2/\Gamma^2 \quad (4)$$

where polydispersity has no units. It is close to zero for monodisperse or nearly monodisperse samples and larger for broader distributions. The hydrodynamic diameters of nanocomplexes were then calculated from D using the Stokes−Einstein equation.[26] All of these measurements were made in triplicate at 25 ± 1 °C.

Electrophoretic Mobility. Electrophoretic mobility (UE) (a particle's velocity in an electric field) for homogeneous and mixed CPP/CS systems was investigated as a function of CS/CPP mass ratio using a Zetasizer Nano-ZS90 instrument (Malvern Instruments, Westborough, MA). All measurements were made in triplicate.

Transmission Electron Microscopy (TEM). The morphological characteristics of the nanocomplexes with increasing CS/CPP mass ratio were examined with a high-performance digital imaging TEM machine (JEOL H-7650, Hitachi High-Technologies Corporation, Tokyo, Japan). One drop of the suspension was stained with 2% (w/v) phosphotungstic acid, placed on a copper grid, and allowed to evaporate in air. Once evaporated, the samples were then placed in the microscope for imaging. The accelerating voltage used was 100 kV, and the images were taken on a Gatan electron energy loss spectrometry system using a 6 eV energy slit.

Fluorescence Spectroscopy. Fluorometric experiments were carried out on a Cary Eclipse fluorescence spectrophotometer (Varian Instruments, Walnut Creek, CA). Various solutions of polymers (0.625−40 μM) were prepared from the 40 μM chitosan stock solution by successive dilution. Samples containing 2 mL of CPP solution and 2 mL of various polymer solutions were mixed to obtain final polymer concentrations of 0.3125−20 μM with a constant CPP content of 2.5 μM. The fluorescence spectra were recorded at excitation and emission wavelengths of λ_{exc} = 280 nm and λ_{emi} = 285−475 nm, respectively. The intensity at 353 nm [tryptophane (Trp)] was used to calculate the binding constant (K) according to literature reports.[27−29]

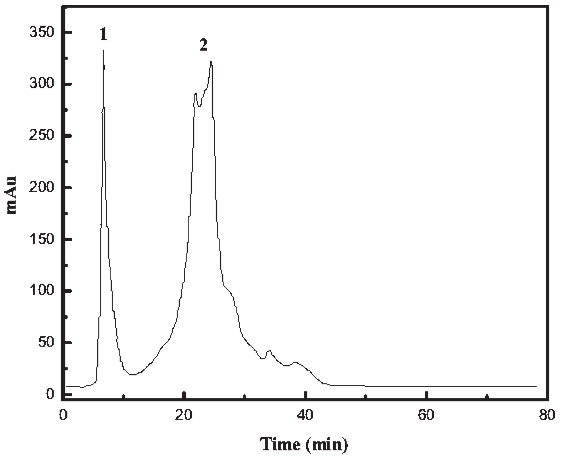

Figure 1. Separation and purification of the hydrolysis peptides by anion-exchange resin column for producing casein phosphopeptides.

RESULTS

Preparation of CPPs. After trypsin hydrolysis of bovine casein and selective precipitation of the hydrolysate at pH 4.6, the soluble peptides were collected for further separation by anion-exchange column. Figure 1 shows the column chromatography of the soluble peptides eluted by mobile phase A and mobile phase B. Positively charged and neutral peptides were directly eluted by mobile phase A (peak 1). The negatively charged peptides, which exchanged with the anion on the gel and absorbed tightly to the column, were eluted by mobile phase B with 1 M NaCl (peak 2). The eluted fractions of negatively charged peptides were collected, desalinated, evaporated, and lyophilized to give the CPP sample.

Chemical Structures of the Peptides. To identify the chemical structures of the peptides interacting with CS, the prepared CS−CPP nanoparticles were dissociated at pH 2.5 because both peptides and chitosan had positive charges. Then, the solution was loaded onto the LC−MS/MS instrument as the analysis sample. Based on the LC−MS/MS data, α_{S1}-, α_{S2}-, and β-casein were identified with high coverage and confidence. The sequence coverage from the LC−MS/MS results is listed in Table 1, with bold underlined characters indicating identified peptides.

The majority of the identified peptides were phosphorylated peptides with different amounts of characteristic clusters of phosphorylated seryl residues, as shown in Figure 2.

Turbidimetric Titration of the Mixture of CPPs and CS. Figure 3 shows turbidimetric titration curves of mixtures of CS and CPPs as a function of pH at 0, 0.0625, 0.125, 0.25, 0.5, and 1 mg/mL CS concentrations (C_{CS}). The turbidities for most of the turbidimetric titration curves were very low and remained

Table 1. Sequence Coverage from LC−MS/MS Results

	CASα1_BOVIN
1	MKLLILTCLV AVALARPKHP IKHQ**GLPQEV LNENL**LRF**FV APFPEVFGKE**
51	**KVNELSKDIG SESTEDQAME DIKQMEAESI SSSEEIVPNS VEQKHIQKED**
101	**VPSERYLGYL EQL**LRLK**KYK VPQLEIVPNS AEERLHSM**KE GIHAQ**QKEPM**
151	**IGVN**QELAY**F YPELFRQF**YQ LDAYPSGAWY YVPLGTQYTD APSFSDIPNP
201	IGSENSEKTT MPLW
	CASβ_BOVIN
1	MKVLILACLV ALALA**RELEE LNVPGEIVES LSSSEESITR INKKIEKFQS**
51	**EEQQQTEDEL QDKIHPF**AQT QS**LVYPFPGP IPN**SLPQN**IP PLTQTPVVVP**
101	**P**FLQPEVMGV SKVKEAMAPK **HKEMPFPKYP VEPF**TESQSL **TLTDVENLHL**
151	**PLPLLQ**SWMH QPHQPL**PPTV MFPPQS**VLS**L SQSKVLPVPQ KAVPYPQRDM**
201	**PIQAFLLYQE PVLGPVRGPF PIIV**
	CASα2_BOVIN
1	MKFFIFTCLL AVALA**KNTME HVSSSEESII SQETYKQEKN MA**INPSKENL
51	CSTFCKEVVR NANEEEYSIG SSSEESAEVA TEEVKITVDD KHYQKALNEI
101	NQF**YQKFPQY** LQYLY**QGPIV LNPWDQVKRN** AVPITPT**LNR EQLSTSEENS**
151	**KKTVDMESTE VFTKKTKLTE EEKNRLNF**LK KISQRYQKFA LPQYLKTVYQ
201	HQKAMKPWIQ PK**TKVIPY**VR YL

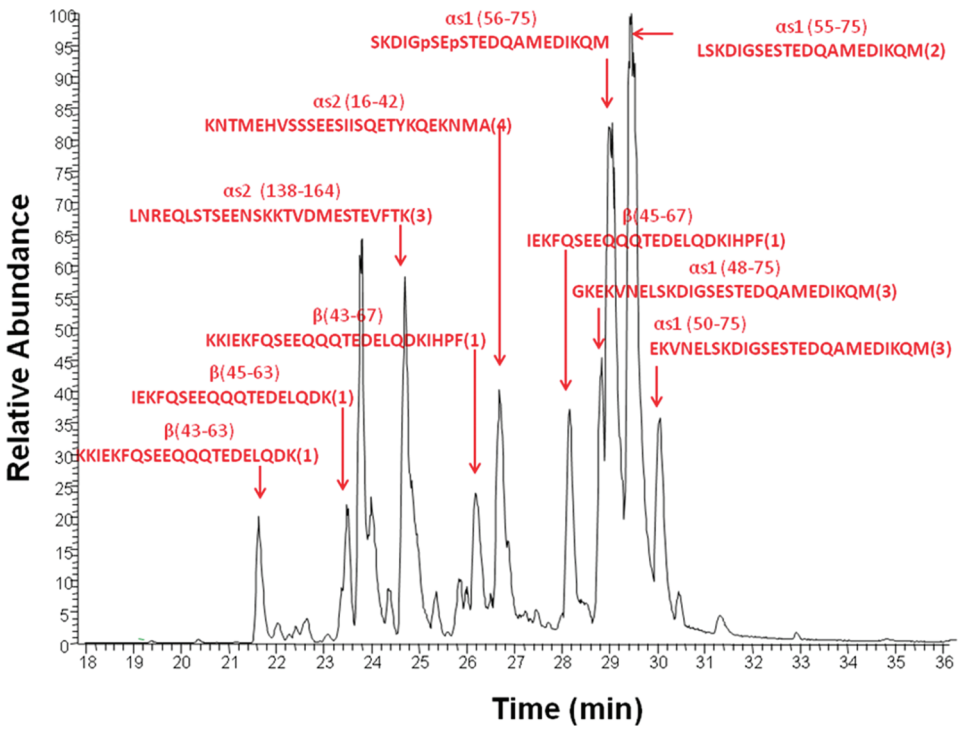

Figure 2. LC−MS/MS base peak chromatogram. Identified peaks are marked. The protein identity, peptide position, and peptide sequences are also labeled. The number of phosphorylation sites is indicated in parentheses if sites were undetermined. Manually confirmed phosphorylation sites are marked in the sequence.

constant until the pH reached a critical value designated as $pH_{\varphi 1}$. All of the curves displayed an abrupt increase in turbidity at $pH_{\varphi 1}$, corresponding to formation of the colloidal complex. At this point, the global phase transition occurred. $pH_{\varphi 1}$ shifted to higher pH values as the CS concentration increased. Nevertheless, further increases in pH made the turbidity change differently in different CS concentration regions. For $C_{CS} \leq$ 0.125 mg/mL, the increasing turbidity reached a maximum at various pH values (pH_{max}) depending on the CS concentration, with lower CS concentrations corresponding to lower pH_{max} value. Beyond pH_{max}, the turbidity decreased steeply with increasing pH and then leveled off at a different threshold ($pH_{\varphi 2}$). For 0.25 mg/mL $\leq C_{CS} \leq$ 1 mg/mL, the decrease in turbidity after the maximum was almost negligible, and $pH_{\varphi 2}$ was

dx.doi.org/10.1021/jp2013557 |J. Phys. Chem. B 2011, 115, 7515–7523

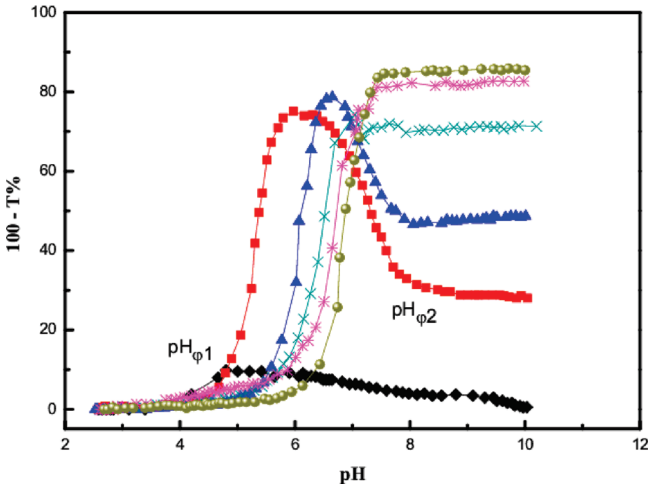

Figure 3. Turbidity [100 − T (%)] as a function of pH for mixtures of 0.5 mg/mL casein phosphopeptide with different concentrations of chitosan in 0.01 M NaCl: (♦) 0, (■) 0.0625, (▲) 0.125, (×) 0.25, (*) 0.5, (●) 1.0 mg/mL chitosan.

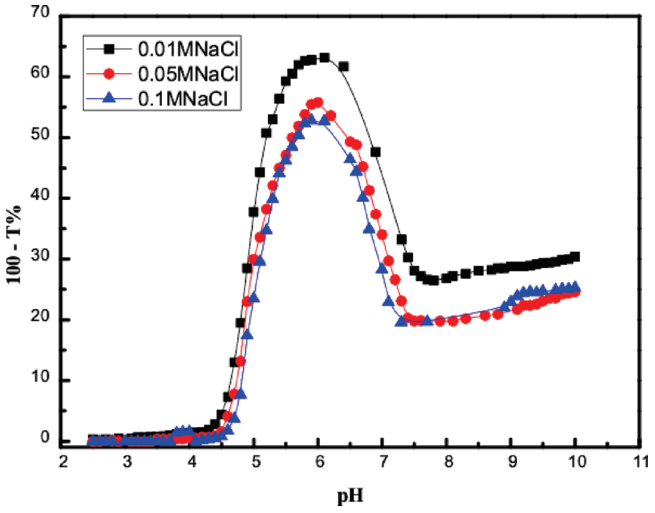

Figure 4. Turbidity [100 − T (%)] as a function of pH for mixtures of 0.5 mg/mL casein phosphopeptide with 0.1 mg/mL chitosan at different concentrations of NaCl: (■) 0.01, (▲) 0.05, (●) 0.1 M.

not observed. Furthermore, floccules were macroscopic in the solution. After 24 h of storage, the turbidity of the mixture of CPPs and CS (0.0625 mg/mL) still remained 22.5%, almost the same as that before storage. However, the turbidity of the sample mixed with 1 mg/mL CS largely declined to 9.2%, and a thick precipitate formed at the bottom of the bottle. Moreover, the effect of the salt concentration on the interaction between the CPPs and CS was studied. Figure 4 shows that no obvious shifts in pH$_{\varphi 1}$ and pH$_{max}$ occurred as the salt concentration was increased from 0.01 to 0.1 M at a CS concentration of 0.1 mg/mL. However, the maximum turbidity of the mixture at pH$_{max}$ decreased with increasing salt concentration.

Dynamic Light Scattering and ζ-Potential Measurements. Figure 5 shows the apparent hydrodynamic diameters and ζ-potentials for the CS−CPP nanoparticles formed as a function of CS/CPP mass ratio at pH 6.0, which is close to the physiological pH. Figure 5A clearly illustrates that both the

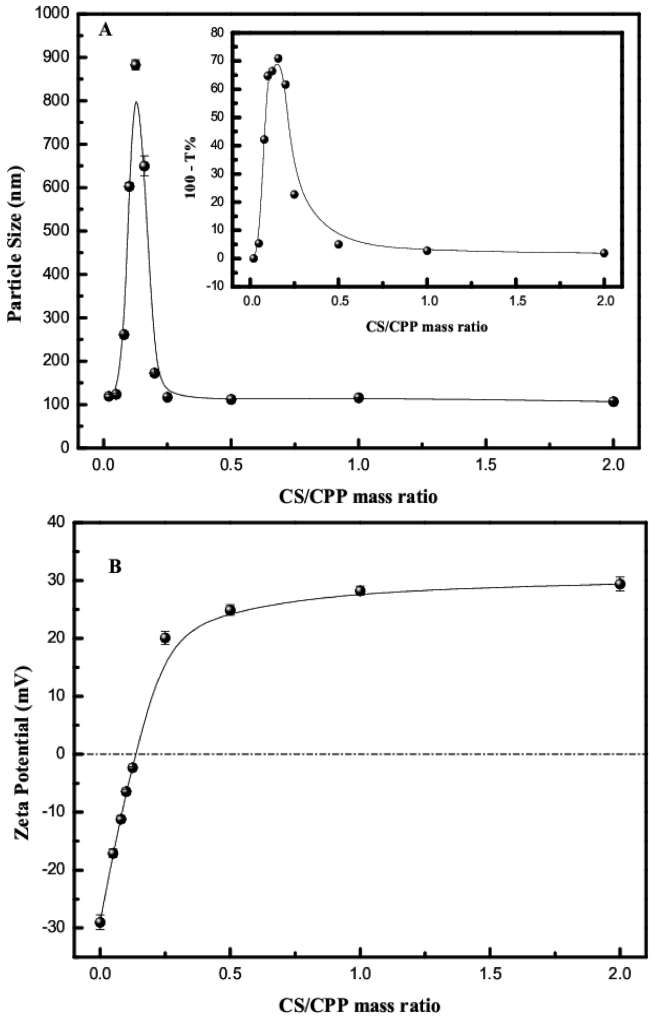

Figure 5. Changes in the (A) mean particle size and (B) ζ-potential of casein phosphopeptide/chitosan nanoparticles with increasing chitosan/casein phosphopeptide mass ratio (the pH of casein phosphopeptide and chitosan are both at pH 6). The inset in part A is the turbidity [100 − T (%)] as a function of different chitosan/casein phosphopeptide mass ratios at pH 6.

particle size and the turbidity had a highly overlapped mass ratio window. In this window, the particle size reached a maximum of 900 nm, and the turbidity reached a peak value with 70% turbidity. In addition, the ζ-potentials changed from negative to positive (Figure 5B), and the position of the peak was close to the neutral point with the ζ-potential value close to zero. Away from the window, the particles had particle sizes of around 115 nm. At the same time, the ζ-potentials of the nanoparticles increased sharply and reached a plateau value at about +29.4 mV. The polydispersity indexes (PDIs) of the nanoparticles ranged from 0.1 to 0.15, indicating a homogeneous dispersion of nanoparticles.

Transmission Electron Microscopy (TEM). TEM was also used to study the distribution of CPPs and CS and the assembly of the nanoparticles. Irregularly shaped CPPNPs were initially observed at a low CS/CPP mass ratio of 0.02 (Figure 6A). When the CS/CPP mass ratio was increased to 0.125, significant bridging of the CPPNPs with CS molecular chains was observed (Figure 6B). When the ratio was further increased to

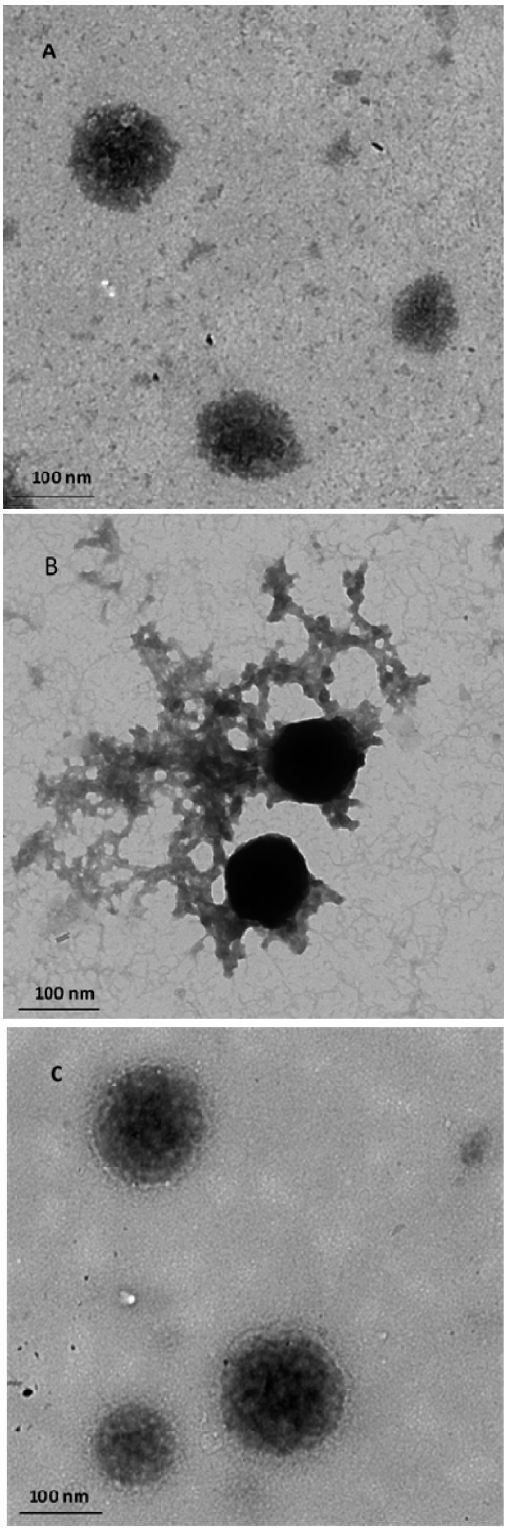

Figure 6. Transmission electron microscopy (TEM) images of the nanocomplexes at chitosan (CS)/casein phosphopeptide (CPP) mass ratios of (A) 0.02, (B) 0.125, and (C) 1. The concentration of CPPs was fixed at 1 mg/mL, and the pH value was 6.

1:1, superfluous CS molecules adsorbed to the surface of the CPPNPs and formed so-called "hairy layers" (Figure 6C). The TEM image of free CS solution was also obtained (data not shown) and was the same as the image of CS molecular chains bridging the CPPNPs.

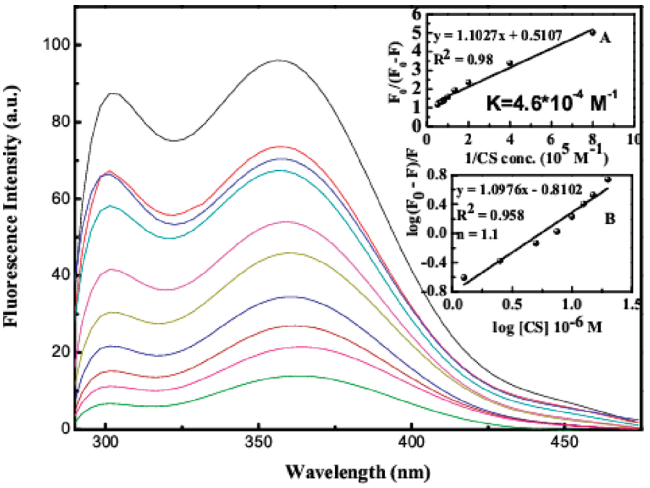

Figure 7. Quenching of the intrinsic fluorescence of casein phosphopeptides by chitosan. Fluorescence emission spectra of the casein phosphopeptide suspension at excitation wavelengths of 280 nm in the presence of (from top to bottom) 0, 0.3125, 1.25, 2.5, 5, 7.5, 10, 12.5, 15, and 20 μM chitosan. Inset A shows the binding constant K_A, which is the ratio of the intercept to the slope for the chitosan−casein phosphopeptide nanocomplex. Inset B shows a plot of $\log[(F_0 - F)/F]$ as a function of log [CS] for the calculation of the number of binding sites.

Fluorescence. The intrinsic fluorescence of proteins, predominantly contributed by Trp residues, has been widely used to investigate the interaction and binding of polysaccharide molecules to proteins in solutions. The fluorescence emission spectra of a CPP suspension in the presence of different concentrations of CS with an excitation wavelength of 280 nm is shown in Figure 7. The intensity of the fluorescence emission of both Tyr (301 nm) and Trp (around 353 nm) residues in the CPPs gradually decreased with increasing CS concentration. No obvious spectral shift was observed for the emission spectra upon polymer−peptide complexation. Trp (W) has already been found inside the peptide amino acid sequence and adjacent to Asp (D), which is the binding site for CS. Therefore, the quenching of Trp fluorescence (353 nm) was selected for monitoring the interaction between the CPPs and the CS and determining the binding constant between the CPPs and CS for CS concentrations ranging from 0.3125 to 20 μM. Lack of fluorescence was interpreted as indicating that a CS−CPP complex had formed.

Under the assumption that the binding of CS molecules to CPPs is a static quenching process, the quenching reaction can be expressed as

$$B + nQ \Leftrightarrow Q_nB \tag{5}$$

where B represents the peptides; Q represents the polysaccharide molecule; n is the number of binding sites; and Q_nB represents the new complex molecule, whose binding constant is K_A. The binding constant (K_A) can be calculated as

$$K_A = \frac{[Q_nB]}{[Q]^n[B]} \tag{6}$$

where [Q] and [B] are the quencher and peptide concentrations, respectively; $[Q_nB]$ is the concentration of nonfluorescent

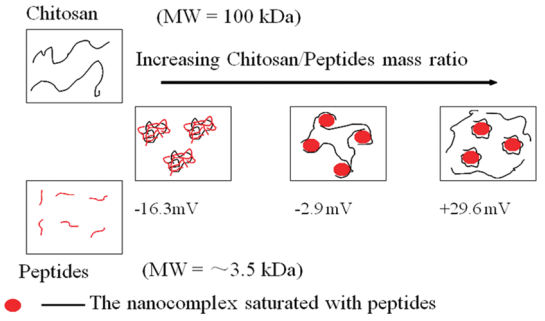

Figure 8. Schematic diagram of the interaction model between chitosan and casein phosphopeptides with increasing chitosan/casein phosphopeptide mass ratio.

fluorophore−quencher complex; and $[B]_0$ is the total peptide concentration

$$[Q_nB] = [B]_0 - [B] \tag{7}$$

$$K_A = \frac{([B]_0 - [B])}{[Q]^n[B]} \tag{8}$$

In a static quenching process, the fluorescence intensity is proportional to the peptide concentration

$$\frac{[B]}{[B]_0} \propto \frac{F}{F_0} \tag{9}$$

The results from the fluorescence measurements can be used to estimate the binding constant of the polymer−peptide complex. From eq 8

$$\log\left[\frac{(F_0 - F)}{F}\right] = \log K_A + n \log [Q] \tag{10}$$

The accessible fluorophore fraction (f) can be calculated by the modified Stern−Volmer equation

$$\frac{F_0}{(F_0 - F)} = \frac{1}{fK[Q]} + \frac{1}{f} \tag{11}$$

where F_0 is the initial fluorescence intensity; F is the fluorescence intensity in the presence of quenching agent (or interacting molecule); K is the Stern−Volmer quenching constant; [Q] is the molar concentration of quencher; and f is the fraction of accessible fluorophore to a polar quencher, which indicates the fractional fluorescence contribution of the total emission for an interaction with a hydrophobic quencher. A plot of $F_0/(F_0 - F)$ versus $1/[Q]$ yields f^{-1} as the intercept on the y axis and $(fK)^{-1}$ as the slope. Thus, the ratio of the ordinate and the slope gives K. A plot $F_0/(F_0 - F)$ versus $1/[CS]$ is shown in the inset of Figure 7. Assuming that the observed change in fluorescence comes from the interaction between CS and CPPs, the quenching constant can be taken as the binding constant of complex formation. The K value reported here is the average of three replicates and three replicate runs for peptide/CS systems, with each run involving several different concentrations of CS (Figure 8). The binding constant was found to be $K_{cs} = 4.6 \times 10^4\ M^{-1}$.

The number of binding sites was calculated from $\log[(F_0 - F)/F] = \log K_A + n \log [CS]$ for static quenching.[30−32] The linear plot of $\log[(F_0 - F)/F]$ as a function of $\log [CS]$ is shown in inset B of Figure 7. The n value from the slope of the straight line was obtained as 1.1.

DISCUSSION

CPPs are a group of negatively charged bioactive peptides. The question of whether all of these peptides participate in binding with CS or whether the interactions between the peptides and CS are specific remained unclear. It was necessary to identify the chemical structure of the peptides that bound to and cross-linked CS. Peptides with different amounts of clusters of phosphorylated seryl residues have already been identified. Based on previous studies,[33,34] in CPPs, the peptide sequences FQSEEQQQTEDELQDK, LSKDIGSESTEDQAMEDIKQM, and DIGSESTEDQAMEDIK play an important role in mineral binding. In addition, the peptide KNTMEHVSSSEESIISQETYKQEKNMA is the key peptide sequence for immunomodulatory activity. All of these bioactive peptide sequences were found in the major CPPs prepared in our study (Figure 2). Therefore, it can be predicted that these nanoparticles assembled from CPPs and CS might serve as biofunctional delivery systems that have bioactivities, such as mineral binding and immunomodulatory activity. Ionic cross-linking of the $-NH_3^+$ groups on CS by the $-PO_4^{3-}$ groups on tripolyphosphate (TPP) has already been used in the preparation of CS nanoparticles for the delivery of protein drugs.[35] Therefore, in the present study, the negatively charged phosphorylated groups in the peptides might also be the dominant binding sites to interact with the positively charged $-NH_3^+$ groups on the CS molecular chain. In addition, the negatively charged amino acids Asp (D) and Glu (E) were found inside the identified peptide sequences. Both of them might also be possible binding sites. In the following discussion, we focused on the details of the interactions between CPPs and CS.

Type 1 turbidimetric titration has been widely used to determine the critical conditions for soluble complexation and phase changes. It is generally accepted that an abrupt change in turbidity arises mainly from a change in either the mass or the size of a complex in the solution.[36,37] The abrupt increase of turbidity at $pH_{\varphi 1}$ denoted the point of a global phase transition, where the cross-linking of CS with CPPs resulted in the formation of insoluble peptide−polysaccharide complexes. It is well-known that electrostatic interactions play an important role in the formation of protein−polysaccharide complexes.[2,38] Increasing the negative net charges of CPPs by increasing the pH would enhance CPP binding to CS, leading to an increase in complex size. The turbidity maximum might be caused by the simultaneous effects of increasing complex size and changing solubility. Before pH_{max}, neutralization of the positive and negative net charges led initially to a loss of solubility, causing a sharp increase in turbidity. After the CS was saturated with bound CPPs, the solubility of the complex increased with further increases in pH because the surface peptides became negatively charged again at higher pH values. The competition of these size and solubility effects caused the maximum in turbidity. Generally speaking, $pH_{\varphi 2}$ was used to denote the dissociation of the protein−polysaccharide complex. Eventually, the remaining turbidity of the mixture with 0.0625 and 0.125 mg/mL CS at pH values higher than $pH_{\varphi 2}$ might mainly be caused by the insolubility of CS in neutral and alkaline pH solutions. CS is readily soluble in dilute acids (pH < 6.0). However, as the pH rose above the pK_a of

the primary amine (pH ≈ 6.3), CS became deprotonated and progressively insoluble.[39]

Interestingly, the $pH_{\varphi 1}$ and pH_{max} values of each curve shifted with the change in CS concentration. The lower the $pH_{\varphi 1}$ value, where CPPs carried less negative charge to interact with positively charged CS, the stronger the tendency for CPPs and CS to form a complex. Lower concentrations of CS with lower amounts of positive surface charges neutralized CPPs more quickly, leading to the appearance of $pH_{\varphi 1}$ and pH_{max} at lower pH values. On the other hand, it is well-known that varying the salt concentration of certain protein/polysaccharide solutions can modify their $pH_{\varphi 1}$ values. For example, low salt concentrations enhance, whereas high salt concentrations inhibit, the tendency toward interactions between proteins and polysaccharides.[40,41] However, according to our results shown in Figure 4, the shifts of $pH_{\varphi 1}$ and pH_{max} were negligibly affected by the salt concentration. The decline of the turbidity strength in Figure 4 as the salt concentration increased from 0.01 to 0.1 M was caused by the screening of the charges of the proteins and polysaccharides, which eventually decreased the mass of the CS/CPP complexes.

Figure 3 also indicates that, with an increase in pH, higher CS concentrations (i.e., 0.25 mg/mL ≤ C_{CS} ≤ 1 mg/mL) caused the disappearance of $pH_{\varphi 2}$. It is known that chitosan is a weak base and is insoluble in neutral and alkaline pH solutions. High CS concentrations thus caused the formation of excess amounts of free CS molecules remaining in the aqueous solution, which would form larger aggregates when the pH was increased to above 7.

Based on the results of turbidimetric titration, pH 6 was selected to investigate the dynamic interaction process between CPPs and CS. Combining the results of DLS, ζ-potential measurements, and TEM, we propose the following interaction model for CPPs and CS complexes, depicted in the schematic diagram in Figure 8. At low CS/CPP mass ratios, negatively charged CPPs easily bind to and cross-link the positively charged CS molecules, partially neutralizing the CS chains by forming negatively charged intrapolymer nanocomplexes saturated with CPPs (CPPNPs).[42] Subsequently, the sharp increase in the particle size with increasing CS/CPP mass ratio can be attributed to the bridging of the nearly neutralized CPPNPs and the formation of associative interpolymer complexes. A further increase in CS concentration causes the formation of positively charged CS−CPP nanocomplexes, and electrostatic repulsion results in the breakdown of the bridges within the associative complexes and the formation of isolated, positively charged spherical CS−CPP nanocomplexes. Furthermore, the electrostatic repulsion between the positively charged CS−CPP nanocomplexes and excess amounts of free CS allow the adsorption of free CS onto the surface of the nanocomplexes and the desorption of CS from the nanocomplexes to reach equilibrium, causing the particle sizes and surface charges of the nanocomplexes to maintain steady values. Similar observations were also found in the addition of cationic chitosan to β-lactoglobulin/pectin multilayer emulsions,[43] as well as micelle−polyelectrolyte coacervation at low salt concentrations.[44]

After hydrolysis of casein, Tyr and Trp were disclosed from the globular protein structure. Therefore, both of their characteristic fluorescence emissions at 301 and 353 nm can been seen in Figure 7. Although both Tyr and Trp were included in the CPPs amino acid sequence, Trp was adjacent to the binding site Asp (D), which should be more sensitive to the binding between CPPs and CS. The quenching of Trp fluorescence (353 nm) was selected to calculate the binding constant. The quenching constant $K_{cs} = 4.6 \times 10^4\ M^{-1}$ suggests a lower affinity of CS−CPP binding than for other ligand−protein complexes.[45] However, there were no obvious changes in the particle size or ζ-potential of the CS−CPP nanocomplexes during the tested 7 days (data not shown), which means that the prepared CS−CPP nanocomplexes are stable and not easily dissociated in solution. Mandeville et al. reported several dendrimers with different amounts of amino groups mainly bound to two fluorophores, Trp-212 buried inside and Trp-134 located on the surface of BSA, through hydrophobic interactions.[27] They also had low binding constants (10^4−$10^5\ M^{-1}$). The f value shown in inset A of Figure 7 suggests that, in addition to electrostatic interactions, CS also interacts with peptides through hydrophobic interactions. However, the emission band at 353 nm showed no obvious shifting upon CS complexation (Figure 7), suggesting that the binding of CS to the peptides did not change the chemical environment around the fluorophore (Trp). Therefore, hydrophobic interactions were not the main driving force during the binding between CS and the peptides. The number of binding sites, $n = 1.1$, suggests that more than one chitosan molecule can bind to the peptides.

CONCLUSIONS

In summary, we have investigated the binding mechanism between CS and CPPs. At low CS/CPP mass ratio, bioactive peptides (CPPs) and chitosan assemble to form new hierarchical nanocomplexes, in which negatively charged CPPs are bound to positively charged CS molecules to form spherical intrapolymer nanocomplexes saturated with CPPs (CPPNPs). Subsequently, the negatively charged CPPNPs are bridged by the added positively charged CS to form significantly larger associative polymer complexes. Further increases in the CS/CPP ratios cause the reversal of the surface charges of the CPPNPs from negative to positive, and the repulsion between the positively charged CPPNPs results in the breakdown of the interpolymer bridges and the formation of isolated positively charged spherical nanocomplexes. The interactions between the peptides and CS are mainly driven by electrostatic interactions with the binding constant $K_{cs} = 4.6 \times 10^4\ M^{-1}$. Hydrophobic interactions also occur during the interaction between CS and CPPs. The phosphorylated groups, Asp, and Glu in the CPPs might be the dominant sites for interaction with the $-NH_3^+$ groups on the CS molecular chains. Detailed chemical structures of peptides incorporating CS were identified using HPLC−MS/MS. The effect of the peptide−CS interaction on the peptide conformation is an important question. Our preliminary circular dichroism (CD) results indicate that the content of β-sheet increased from 17% to 40% upon binding to chitosan. This suggests that peptide unfolding might occur during the chitosan−peptide interaction process. Further studies are still underway in our laboratories. This study provides a simple and efficient way to prepare biopolymer nanocomplexes that can be used for the encapsulation and delivery of peptides and enzyme. In addition, it represents a new approach for preparing CS nanoparticles with biofunctionality.

AUTHOR INFORMATION

Corresponding Author

*Tel.: +86 25 84396791 (X.X.Z.), 732-932-7193 (Q.R.H.). E-mail: zengxx@njau.edu.cn (X.X.Z.), qhuang@aesop.rutgers.edu (Q.R.H.).

■ ACKNOWLEDGMENT

We thank H. Y. Zheng and M. Q. Qian for technical assistance in LC−MS/MS measurements. This work was supported by the U.S. Department of Agriculture National Research Initiative (Grant 2009-35603-05071, Q.H.) and a Grant-in-Aid from the 863 Program, Ministry of Science and Technology, People's Republic of China (2007AA10Z351 and 2007AA100403).

■ REFERENCES

(1) Caruso, F.; Mohwald, H. *J. Am. Chem. Soc.* **1999**, *121*, 6039–6046.
(2) Cooper, C. L.; Dubin, P. L.; Kayitmazer, A. B.; Turksen, S. *Curr. Opin. Colloid Interface Sci.* **2005**, *10*, 52–78.
(3) de Kruif, C. G.; Weinbreck, F.; de Vries, R. *Curr. Opin. Colloid Interface Sci.* **2004**, *9*, 340–349.
(4) Hamidi, M.; Azadi, A.; Rafiei, P. *Adv. Drug Deliv. Rev.* **2008**, *60*, 1638–1649.
(5) Burgess, D. J.; Dubin, P. L.; Bock, J.; Davies, R. M.; Schulz, D. N.; Thies, C. *Macromolecular Complexes in Chemistry and Biology*; Springer-Verlag: Berlin, 1994.
(6) Chan, C.; Burrows, L. L.; Deber, C. M. *J. Biol. Chem.* **2004**, *279*, 38749–38754.
(7) Kuo, H. H.; Chan, C.; Burrows, L. L.; Deber, C. M. *Chem. Biol. Drug Des.* **2007**, *69*, 405–412.
(8) Shoichet, M. S. *Macromolecules* **2010**, *43*, 581–591.
(9) Kuschert, G. S. V.; Coulin, F.; Power, C. A.; Proudfoot, A. E. I.; Hubbard, R. E.; Hoogewerf, A. J.; Wells, T. N. C. *Biochemistry* **1999**, *38*, 12959–12968.
(10) Rusnati, M.; Coltrini, D.; Oreste, P.; Zoppetti, G.; Albini, A.; Noonan, D.; Faagagna, F. A.; Giacca, M.; Prestai, M. *J. Biol. Chem.* **1997**, *272*, 11313–11320.
(11) Donald, A. *Nat. Mater.* **2004**, *3*, 579–581.
(12) Mezzenga, R.; Schurtenberger, P.; Burbidge, A.; Michel, M. *Nat. Mater.* **2005**, *4*, 729–740.
(13) Ubbink, J.; Burbidge, A.; Mezzenga, R. *Soft Mater.* **2008**, *4*, 1569–1581.
(14) Hartmann, R.; Meisel, H. *Curr. Opin. Biotechnol.* **2007**, *18*, 163–169.
(15) Su, R. X.; Qi, W.; He, Z. M.; Yuan, S. X.; Zhang, Y. B. *Food Chem.* **2007**, *104*, 276–286.
(16) Erba, D.; Ciappellano, S.; Testolin, G. *Nutrition* **2002**, *18*, 743–746.
(17) Cross, K. J.; Huq, N. L.; Palamara, J. E.; Perich, J. W.; Reynolds, E. C. *J. Biol. Chem.* **2005**, *280*, 15362–15369.
(18) Laparra, J. M.; Alegria, A.; Barbera, R.; Farre, R. *Food Res. Int.* **2008**, *41*, 773–779.
(19) Kampa, M.; Loukas, S.; Hatzoglou, A.; Daminaki, A.; Martin, P. M.; Castanas, E. *Eur. J. Pharmacol.* **1997**, *335*, 255–265.
(20) Hata, I.; Higashiyama, S.; Otani, H. *J. Dairy Res.* **1998**, *65*, 569–578.
(21) Qi, L. F.; Xu, Z. R.; Jiang, X.; Hu, C. H.; Zou, X. F. *Carbohydr. Res.* **2004**, *339*, 2693–2700.
(22) Qi, L. F.; Xu, Z. R. *Bioorg. Med. Chem. Lett.* **2006**, *16*, 4243–4245.
(23) Bowman, K.; Leong, K. W. *Int. J. Nanomed.* **2006**, *1*, 117–128.
(24) Agnihotri, S. A.; Mallikarjuna, N. N.; Aminabhavi, T. M. *J. Controlled Release* **2004**, *100*, 5–28.
(25) Ellegård, K. H.; Gammelgård-Larsen, C.; Sørensen, E. S.; Fedosov, S. *Int. Dairy J.* **1999**, *9*, 639–652.
(26) Brown, W. *Dynamic Light Scattering: The Method and Some Applications*; Oxford University Press: Oxford, U.K., 1993; pp 177−241.
(27) Mandeville, J. S.; Tajmir-Riahi, H. A. *Biomacromolecules* **2010**, *11*, 465–472.
(28) Bi, S.; Ding, L.; Tian, Y.; Song, D.; Zhou, X.; Liu, X.; Zhang, H. J. *J. Mol. Struct.* **2005**, *703*, 37–45.
(29) Dufour, C.; Dangles, O. *Biochim. Biophys. Acta* **2005**, *1721*, 164–173.
(30) Charbonneau, D.; Beauregard, M.; Tajmir-Riahi, H. A. *J. Phys. Chem. B* **2009**, *113*, 1777–1784.
(31) Liang, L.; Tajmir-Riahi, H. A.; Subirade, M. *Biomacromolecules* **2008**, *9*, 50–55.
(32) Huang, B. X.; Dass, C.; Kim, Y.-H. *Biochem. J.* **2005**, *387*, 695–702.
(33) Meisel, H.; FitzGerald, R. J. *Curr. Pharm. Des.* **2003**, *9*, 1289–1295.
(34) Silva, S. V.; Malcata, F. X. *Int. Dairy J.* **2005**, *15*, 1–15.
(35) Hu, B.; Pan, C. L.; Sun, Y.; Hou, Z. Y.; Ye, H.; Hu, B.; Zeng, X. X. *J. Agric. Food Chem.* **2008**, *56*, 7451–7458.
(36) Xia, J. L.; Dubin, P. L.; Dautzenberg, H. *Langmuir* **1993**, *9*, 2015–2019.
(37) Jiang, H. L.; Zhu, K. J. *J. Appl. Polym. Sci.* **2001**, *80*, 1416–1425.
(38) Laos, K.; Brownsey, G. J.; Ring, S. G. *Carbohydr. Polym.* **2007**, *67*, 116–123.
(39) Pillai, C. K. S.; Paul, W.; Sharma, C. P. *Prog. Polym. Sci.* **2009**, *34*, 641–678.
(40) Wang, X. Y.; Wang, Y. W.; Ruengruglikit, C.; Huang, Q. R. *J. Agric. Food Chem.* **2007**, *55*, 10432–10436.
(41) Seyrek, E.; Dubin, P. L.; Tribet, C.; Gamble, E. A. *Biomacromolecules* **2003**, *4*, 273–282.
(42) Xia, J. L.; Zhang, H. W.; Rigsbee, D. R.; Dubin, P. L.; Shaikh, T. *Macromolecules* **1993**, *26*, 2759–2766.
(43) Guzey, D.; McClements, D. J. *Adv. Colloid Interface Sci.* **2006**, *128−130*, 227–248.
(44) Wang, Y.; Kimura, K.; Huang, Q. R.; Dubin, P. L.; Jaeger, W. *Macromolecules* **1999**, *32*, 7128–7134.
(45) Kratochwil, N. A.; Huber, W.; Muller, F.; Kansy, M.; Gerber, P. R. *Biochem. Pharmacol.* **2002**, *64*, 1355–1374.